A STUDY OF TURBULENT FLOWS IN 2-D CHANNELS USING LARGE EDDY SIMULATIONS

Luiz Augusto C. A. Schiavo
Antonio Batista de Jesus
Instituto Tecnológico de Aeronáutica, DCTA/ITA, Brazil
augustoschiavo@gmail.com, antoniobjota@gmail.com

William Roberto Wolf
Universidade de Campinas, UNICAMP, Brazil
wolf@fem.unicamp.br

João Luiz F. Azevedo
Instituto de Aeronáutica e Espaço, DCTA/IAE/ALA, Brazil
joaoluiz.azevedo@gmail.com

Abstract. Large eddy simulation (LES) has been used to study turbulence, aeroacoustics and combustion. In the present work, LES studies have been performed for low and moderate Reynolds number channel flows, using an incompressible formulation and the WALE sub-grid scale model. In LES, the larger scales are resolved and the small scales are modeled by a subscale model. The advantage of this type of simulation is the behavior of the large scales is extremely affected by the topology of the flow under analysis. In this context, the main objective of this work is to study flows near walls, in channels with curvature, to evaluate the effect of adverse pressure gradients in the flow wall friction and pressure coefficients. The work presents comparative results between LES and Reynolds-averaged Navier-Stokes (RANS) calculations. The RANS turbulence models are not able to capture the full physics of turbulence related with adverse pressure gradients. Such limitations are observed both in separated and attached flow conditions in the adverse pressure gradient regions, and they seem to be related to an incorrect account for the evolution of the turbulent kinetic energy close to the walls.

Keywords: LES, Channel flows, Turbulent flows, Turbulence models

1. INTRODUCTION

The resolution of the Navier-Stokes equations without any type of modeling of the turbulent scales is known as DNS (Direct Numerical Simulation). This type of simulation requires a very high computational capability in order to represent all turbulence scales. This type of simulation is of great value in the study of turbulence. However, it requires computational meshes that are able to "see" the smallest turbulent scales present in the flow, *i.e.*, the Kolmogorov scales. This leads to very stringent requirements in terms of mesh refinement and, hence, this approach becomes impractical for moderate and high Reynolds numbers for any modestly complex configuration.

The next level of formulation is known as large eddy simulation (LES), and it has been used to study turbulence, aeroacoustics and combustion. In LES, the larger scales are resolved and the small scales are modeled by a subscale model. One of the advantages of this type of formulation is that the behavior of the large scales is extremely affected by the topology of the flow under analysis, whereas the small scales have a universal behavior. Moreover, since the small scales are modeled, mesh requirements are much less stringent in LES and, therefore, it is already possible to address moderate Reynolds number flows for some practical configurations.

The formulation in which all turbulent scales are modeled consists in the Reynolds-averaged Navier-Stokes (RANS) equations. Mesh requirements for the RANS formulation are, therefore, much less severe than for LES. Consequently, RANS modeling became the workhorse of the industry, having acceptable computational cost to treat real engineering problems. On the other hand, the development of more accurate turbulence models is an open topic in RANS formulations. Much effort has been concentrated in the capability of predicting flow separation due to adverse pressure gradients and this is probably one of the reasons of the huge success found by the SST turbulence model in the aerospace industry (Menter *et al.*, 2003). In aerospace, mechanical, naval and many others engineering areas, drag prediction of a component is an important step of an engineering project. For an aircraft project, the prediction of separated flow and adverse pressure gradient regions is fundamental to obtain a good result for the drag.

In the present work, LES studies have been performed for low and moderate Reynolds number channel flows, using an incompressible formulation and the WALE sub-grid scale model. In this context, the main objective of this work is to evaluate the effect of adverse pressure gradients in the flow wall friction and pressure coefficients. The work presents comparative results between LES and RANS calculations. In the domain of RANS modeling, it is found that, despite recent improvements, the turbulence models are still not capable of adequately predicting the flow characteristics in

ISSN 2176-5480

L.A.C.A. Schiavo, A.B. Jesus, W.R. Wolf and J.L.F. Azevedo
A Study of Turbulent Flows in 2-D Channels Using Large Eddy Simulations

adverse pressure gradient (APG) regions (Jesus *et al.*, 2013; Jeyapaul and Rumsey, 2013). Two-equation models tend to either under-predict or over-predict flow separation. Reynolds stress transport models show better results, especially in the pressure distribution. However, none of the RANS models proved to be fully accurate in skin friction calculations. The inaccuracies of RANS models in APG regions have been associated with the inability of such models of correctly predicting flow separation and re-attachment locations (Menter *et al.*, 2003; Jeyapaul and Rumsey, 2013). On the other hand, recent studies (Jesus *et al.*, 2013) suggest that the behavior of the skin friction coefficient in APG regions of smooth bumps does not depend on flow separation. In other words, the behavior in either attached or mildly separated flow is very similar, indicating that the prevailing physical mechanism is mostly associated to the adverse pressure gradient condition.

The present work aims at extending the previous study (Jesus *et al.*, 2013) through the consideration of higher Reynolds number flows, for which there is no DNS data for comparison. The geometric configuration addressed consists of a 2-D bump in a channel, which is described in detail in Jesus *et al.* (2013). One of the differences with regard to the previous investigation is that the Reynolds number is increased up to $Re_\tau = 2000$ based on the friction velocity at the channel inlet. This is a case of particular interest as there is no flow separation on the downstream portion of the bump. In addition, previous LES calculations performed at $Re_\tau = 950$ are reworked using finer meshes. LES results are compared to the corresponding RANS solutions using two-equation and seven equation models. Comparison is initially performed in terms of skin friction and pressure coefficient distributions, followed by a deeper analysis of turbulent kinetic energy and Reynolds stress budgets.

As in the previous study (Jesus *et al.*, 2013), LES calculations use the MFLOPS3D semi-spectral code, developed at Laboratoire de Mécanique de Lille (LML). The Wall-Adapting Local Eddy-viscosity (WALE) closure (Nicoud and Ducros, 1999) is used to model the sub-filter stresses. RANS computations are performed using the Ansys Fluent v.14.0 commercial code, with two different two-equation models, namely, realizable k-ϵ and SST models, and the Reynolds stress transport model (RSM) available in Ansys Fluent (2011). In the present manuscript, the formulation and problem definition are discussed, followed by the presentation of LES results, including those at $Re_\tau = 617$, 950 and 2000, and the corresponding comparison with RANS solutions.

2. GEOMETRIC AND PHYSICAL MODELS

2.1 Bump Geometry

The bump profile under study is displayed in Fig. 1. It combines an initial favorable pressure gradient region in the upstream portion of the bump with an APG region in the back of it. This bump profile was studied both in wind-tunnel experiments, at high Reynolds numbers, and by DNS calculations (Marquillie *et al.*, 2008, 2011), at low Reynolds numbers, $Re_\tau = 395$ and 617, during the recent WALLTURB European project (Stanislas *et al.*, 2009). For all calculations performed here, as well as in the DNS computations, the bump is considered as installed in a channel with 2.0 m in height and 4π m in length.
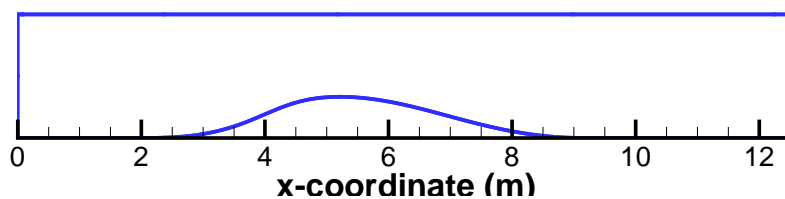

Figure 1. Bump geometry.

2.2 LES Formulation

LES computations are performed using the MFLOPS3D code developed at the LML. This is a semi-spectral code, developed for the study of boundary layer or channel flows around two-dimensional bumps. The code has been used for performing laminar flow instability computations (Marquillie and Ehrenstein, 2003), DNS of turbulent channel flows around two-dimensional bumps (Marquillie *et al.*, 2008, 2011), and LES of the same types of flows (Kuban *et al.*, 2012). The code, when running in LES mode, solves the filtered incompressible Navier-Stokes equations, which can be given by

$$\frac{\partial \vec{\bar{u}}}{\partial t} + \left(\vec{\bar{u}} \cdot \vec{\nabla} \right) \vec{\bar{u}} = -\vec{\nabla}\bar{p} + \frac{1}{Re}\bar{\Delta}\vec{\bar{u}} - \vec{\nabla} \cdot \tau^{sfs} \tag{1}$$

$$\vec{\nabla} \cdot \vec{\bar{u}} = 0 \tag{2}$$

where Eqs. (1) and (2) represent the momentum equations and mass conservation, respectively. The three-dimensional filtered velocity vector is identified here as

$$\vec{u} = \left\{ \begin{array}{c} \bar{u} \\ \bar{v} \\ \bar{w} \end{array} \right\} , \qquad (3)$$

or as $\bar{u}_i$ in indicial notation. The sub-filter stresses are defined as

$$\tau_{ij}^{sfs} = \overline{u_i u_j} - \bar{u}_i \bar{u}_j . \qquad (4)$$

In the present work, sub-filter terms are evaluated using the WALE model (Nicoud and Ducros, 1999), which is very adequate for wall bounded flow computations as it was conceived to recover the correct eddy-viscosity near wall scaling without the need for an explicit damping.

The MFLOPS3D code uses a variable transformation that maps the physical domain, shown in Fig. 1, into a Cartesian domain. The mapping coordinates are given by

$$y = \frac{1}{L}\left(1 - \gamma\left(x\right)\right)y + \gamma(x) \qquad , \qquad \gamma(x) = \frac{L + \eta(x)}{\eta(x) - L} , \qquad (5)$$

where L and $\eta(x)$ are the channel height and the graph of the bump in physical coordinates, respectively. With the coordinates defined in Eq. (5), the gradient, Laplacian and divergent operators in the Navier-Stokes equations are re-written, and the resulting equations can be expressed as

$$\frac{\partial \vec{u}}{\partial t} + \left(\vec{u} \cdot \vec{\nabla}_\eta\right)\vec{u} + \left(\vec{u} \cdot \vec{G}_\eta\right)\vec{u} = -\vec{\nabla}_\eta p - \vec{G}_\eta p + \frac{1}{Re}\Delta_\eta \vec{u} + \frac{1}{Re}L_\eta \vec{u} \qquad -\vec{\nabla}_\eta \cdot \tau^{sfs} - \vec{G}_\eta \cdot \tau^{sfs} \qquad (6)$$

$$\vec{\nabla}_\eta \cdot \vec{u} + \vec{G}_\eta \cdot \vec{u} = 0 \qquad (7)$$

Here, $\vec{\nabla}_\eta$ represents the Cartesian components of the transformed gradient operator and $\vec{G}_\eta$ includes the terms of the gradient operator involving the bump profile. Similarly, Δ_η contains the Cartesian terms of the transformed Laplacian operator, and L_η groups the terms associated to the bump profile and its derivative. Equations (6) and (7) are the transformed momentum and mass conservation equations, which are solved as part of the numerical procedure to be described in the forthcoming paragraphs.

The transformed Navier-Stokes equations are discretized using fourth-order finite differences in the streamwise direction, while Chebyshev polynomials are employed in the normal direction. A Fourier transform is performed in the spanwise direction, which is assumed periodic. Time integration is performed using an implicit second-order backward Euler method for the terms containing the Cartesian components of the Laplacian operator, while an explicit second-order Adams-Bashforth method is used for all other terms, including the sub-filter stresses. Pressure-velocity coupling is achieved by a fractional-step method which performs an iterative process. In this process, the solution of the momentum equations yield an intermediate velocity field, whereas the solution of the pressure Poisson equation determines an intermediate pressure. Afterwards, iterations based on the continuity equation are used in order to obtain a pressure correction that produces a divergent-free velocity field. Computations are performed in Fourier space, and each Fourier mode is solved independently using parallel computations. The nonlinear and sub-filter terms are computed in physical space. The computational process is parallelized by mesh partition and the Message Passing Interface (MPI) protocol is used to communicate between processors.

Further details of the transformed equations and numerical methodology can be found in previous work which uses the MFLOPS3D code (Marquillie *et al.*, 2008). Boundary conditions for the inlet flow are obtained from a precursory periodic channel flow computation. No-slip conditions are imposed at the top and bottom walls, and the spanwise direction is assumed periodic with a π m width. The outflow boundary of the computational domain is treated as a convective boundary with uniform velocity, *i.e.*, the velocity vector is assumed to be transported by a constant convective velocity, U_c, as

$$\frac{\partial \vec{u}}{\partial t} + U_c \frac{\partial \vec{u}}{\partial x} = 0 . \qquad (8)$$

2.3 RANS Formulation

RANS calculations are performed using the Ansys Fluent v.14.0 commercial CFD package. Two 2-equation turbulence models, namely, realizable k-ϵ (Shih *et al.*, 1995) and SST (Menter *et al.*, 2003) models, are evaluated along with one of the Reynolds stress transport models (RSM) available in the code (Launder and Shima, 1989). The steady-state, two-dimensional, incompressible pressure-based solver, SIMPLE method, is used with the default settings of the Fluent package. At the walls, the realizable k-ϵ and the RSM calculations use the so-called enhanced wall treatment option,

which employs a two-layer formulation for the near wall region. Hence, in this region, the length scales used to compute the turbulent viscosity and the turbulent dissipation (ϵ) are adjusted to take into account the effects of the wall proximity (Ansys Fluent, 2011). In addition, the RSM model specifies values for the Reynolds stresses, in the first cell off the wall, through the use of the log-law and the assumption of equilibrium (Ansys Fluent, 2011).

Similarly to the LES computations, a precursory periodic channel flow is run to generate inlet conditions that are used for the calculations with the bump in the channel. No-slip conditions are imposed at the walls and a constant pressure is assumed at the outlet. A two-dimensional mesh with 400×100 quadrilaterals in the streamwise and wall-normal directions, respectively, is used for the RANS calculations over the bump under study. Figure 2 shows the mesh used for RANS computations. The centroid of the first off-the-wall cell is placed at 0.25 mm from the wall, which approximately corresponds to a maximum $y^+ = 0.3$ for the present calculations.

Figure 2. Overall view of the RANS mesh.

3. RESULTS

LES computations at $Re_\tau = 617,\ 950$ and 2000 are performed. Periodic channel flows, at the same Reynolds numbers, are computed and, after statistical convergence, the velocity vectors at a plane normal to the streamwise direction are stored for the equivalent of two flow-through times, for each case. Such velocity history is imposed as entrance condition at the inlet for the bump calculations. Computations at $Re_\tau = 617$ use 320×129 nodes in the streamwise and normal directions, respectively, and 128 Fourier modes in the spanwise direction. Similarly, simulations at $Re_\tau = 950$ employ 448×97 grid points in the streamwise and normal directions, and, again, 128 modes in the spanwise direction. Computations at $Re_\tau = 2000$ used a finer mesh with 1024×193 grid points in the streamwise and normal directions, and 256 modes in the spanwise direction. A time step of 0.001 sec is used in all cases. It should be noticed that the mesh refinement levels used here are beyond those adopted in previous LES calculations with the same code and which showed good comparison with DNS (Kuban *et al.*, 2012).

Figure 3 presents the LES-calculated skin friction coefficient distributions at the bottom wall for the Reynolds numbers under study. Similarly, Fig. 4 brings the corresponding pressure coefficient distributions at the same Reynolds numbers. One can see that LES results at $Re_\tau = 617$ show good comparison with those obtained from DNS. At this Reynolds number, LES calculations show a small separation region at the top of the bump, followed by flow re-attachment still over the bump. Such result, again, is completely consistent with the DNS calculations. In both DNS and LES results, it can be seen that, after the initial decrease in the skin friction coefficient in the rear part of the bump, a strong recovery of C_f is observed downstream of the separated flow region. LES results tend to slightly under-predict the skin friction coefficient at the re-attachment region when compared to DNS values.

At $Re_\tau = 950$, it can be noticed that the separation region on the bottom wall is smaller than that in the $Re_\tau = 617$ computations. In the re-attachment region, a strong recovery of the friction coefficient is again observed, similar to what is seen in the $Re_\tau = 617$ results. At $Re_\tau = 2000$, the skin friction distribution has a similar pattern to those obtained in the lower Reynolds number cases. A similar rapid decrease and recovery of C_f in the APG region is observed, but there is no flow separation. This latter result is an indication that the turbulence physics in the APG region seems to be related not only to flow separation, but also to existence of an adverse pressure gradient region itself. The pressure coefficient distributions, presented in Fig. 4, show again a very good comparison between LES and DNS at $Re_\tau = 617$. At higher Reynolds numbers, pressure distributions are similar up to the suction peak. At the downstream portion of the bump, an inflection in the pressure coefficient distribution can be observed, which seems to be related to the extension of the separated flow region. This feature is not observed at the $Re_\tau = 2000$ results.

In order to assess the behavior of RANS models, Figs. 5 and 6 compare the friction and pressure coefficient distributions, respectively, along the bottom wall, obtained from RANS computations and DNS at $Re_\tau = 617$. It can be seen that, in the favorable pressure gradient region, the RANS results have a very good agreement with the DNS data. However, this behavior does not hold for the adverse pressure gradient region. The realizable k-ϵ model captures the drop in friction coefficient due to the adverse pressure gradient, but it does not show any flow separation. Moreover, downstream of the bump, the friction coefficient slowly recovers towards a constant value. The SST results compare very well with DNS up to the separation point. This is an expected result as this model is widely known to predict flow separation better than k-ϵ models (Menter *et al.*, 2003).
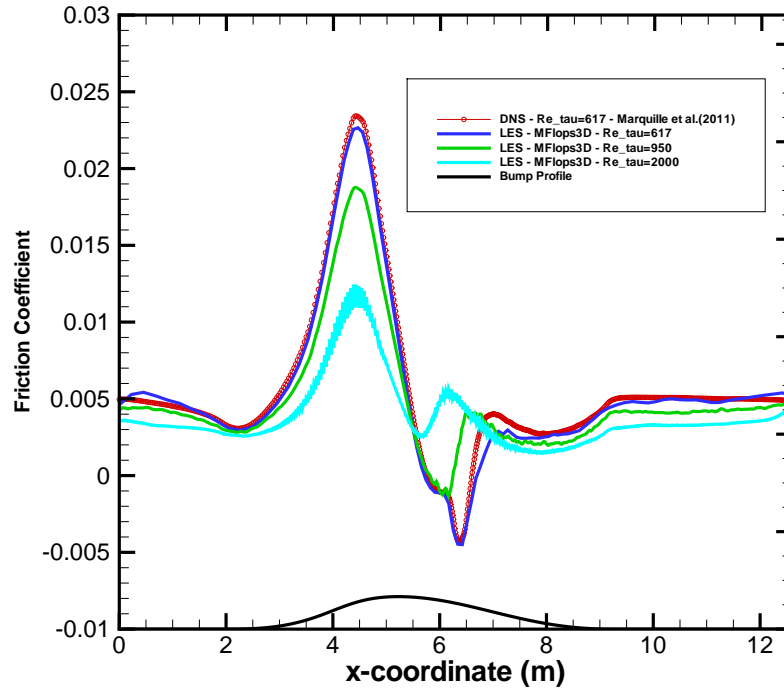
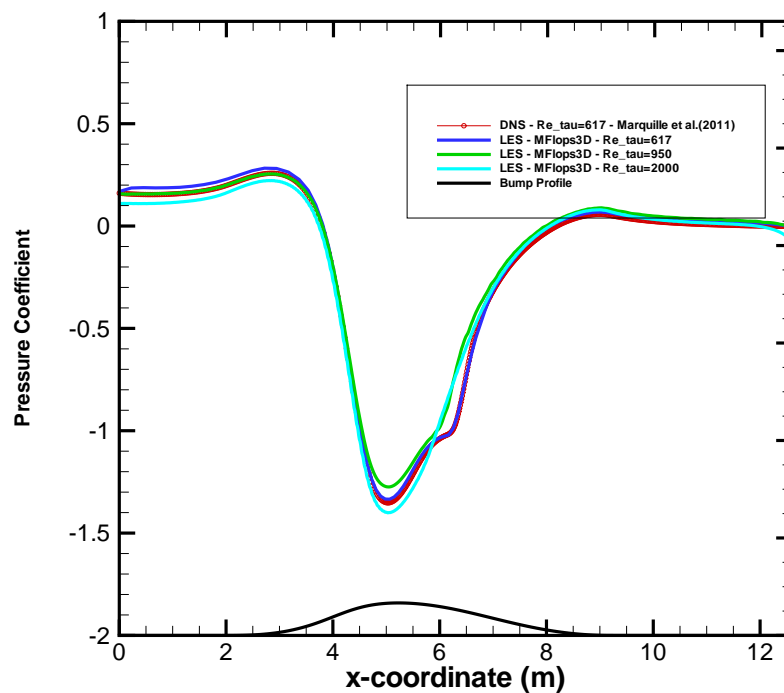Figure 3. Bottom wall friction coefficient distributions. LES: $Re_\tau = 617$, 950 and 2000; DNS: $Re_\tau = 617$.

Figure 4. Bottom wall pressure coefficient distributions. LES: $Re_\tau = 617$, 950 and 2000; DNS: $Re_\tau = 617$.
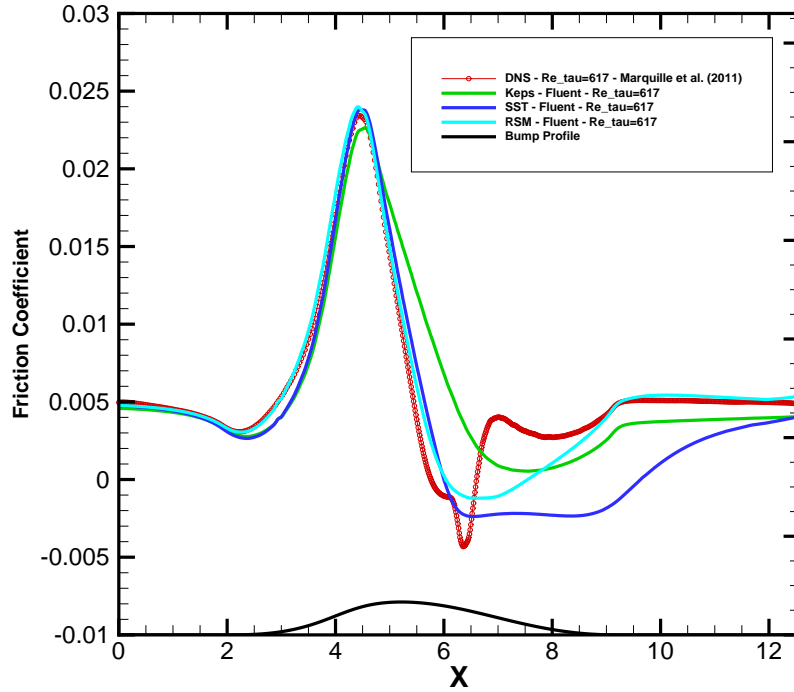
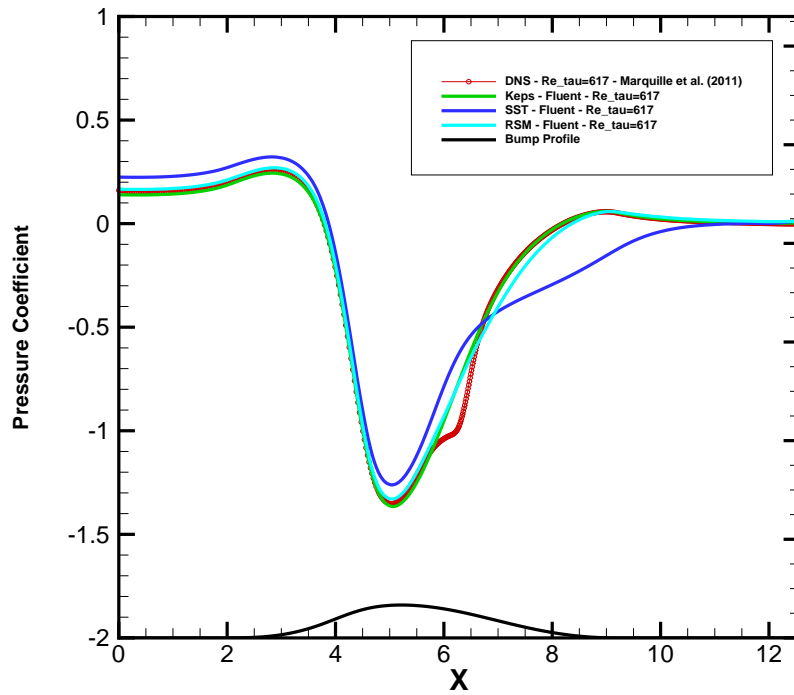Figure 5. Bottom wall friction coefficient distributions. RANS: $Re_\tau = 617$; DNS: $Re_\tau = 617$.

Figure 6. Bottom wall pressure coefficient distributions. RANS: $Re_\tau = 617$; DNS: $Re_\tau = 617$.

Downstream of the separation point, however, a much larger separation bubble, than what is seen in DNS, is formed and flow re-attachment only occurs downstream of the bump, with the slow recovery of the friction coefficient. The RSM model has a performance similar to that of the SST model up to the separation point. After separation, the recovery of the skin friction coefficient is slower than the one present in the DNS results, with a larger separation bubble. However, when compared to the two-equation model results, it can be seen that the RSM model yields a better comparison with DNS. When compared to the LES results, it can be noticed that none of the RANS models correctly predicts either the negative peak of the skin friction at the separated flow region or its recovery after reattachment. In terms of pressure coefficients, Fig. 6 shows that RANS models do not correctly predict the inflection observed in DNS results for the pressure coefficient distribution in the separated flow region.

Figures 7 and 8 present skin friction and pressure coefficient distributions, respectively, along the bottom wall for the RANS and LES calculations at $Re_\tau = 950$. Similar trends as those observed in the $Re_\tau = 617$ calculations can be noticed in the present case. All RANS models produce results very similar to DNS in the favorable pressure gradient region. In the APG region, the realizable k-ϵ model does not predict either the decrease or the rise in skin friction values observed in LES results. The SST model predicts a large flow separation region, missing slightly the separation point position. As one can see in Fig. 7, the SST results for C_f indicate separation slightly downstream of the separation point predicted by the LES calculations. However, the reattachment point occurs downstream of the bump, which is in dramatic contrast with the LES results. The RSM calculation presents the best results in terms of skin friction distribution, despite the fact that it does not predict any flow separation or the sharp rise in C_f in the flow reattachment region. None of the RANS models captures all the details of the pressure coefficient distribution, but the predictions from k-ϵ and RSM closures appear to be in better agreement with LES results than the SST calculation.

Figures 9 and 10 present the corresponding skin friction and pressure coefficient distributions from RANS and LES solutions at $Re_\tau = 2000$. At this Reynolds number, flow separation in the downstream portion of the bump does not occur, according to the present LES calculations. Nevertheless, rapid decrease and recovery of skin friction coefficient in the APG region is still observed, similar to the behavior observed for lower Reynolds numbers. RANS models continue to produce results very similar to LES in the zero or favorable pressure gradient regions. In the APG region, the realizable k-ϵ model does not reproduce either the slope or the levels of skin friction observed in LES results. The SST model also misses the skin friction rapid decrease and it still predicts some flow separation at the rear of the bump. The RSM calculations present the best results in terms of skin friction coefficient distribution, with a better relative performance than observed for the lower Reynolds number calculations. The initial decrease of C_f in the APG region is well capture and, despite not predicting the full drop of the friction coefficient, the change in slope in the distribution at the rear portion of the bump and its recovery are well predicted. The superiority of RSM results relative to those obtained with two-equation models can also be observed in Fig.10, in terms of the pressure coefficient distributions.

In the literature, as discussed, the difficulties of RANS models in predicting skin-friction coefficient distributions in APG regions have commonly be attributed to the inability of correctly predicting flow separation and reattachment locations and the physics of turbulence associated with separation phenomena (Jeyapaul and Rumsey, 2013). However, DNS results (Marquillie *et al.*, 2011) have shown strong peaks of turbulent kinetic energy associated with adverse pressure gradient regions. Furthermore, other studies (Kuban *et al.*, 2012), performed with the same CFD code here used, have indicated that those peaks are also present in LES results. On the other hand, such peaks are not correctly predicted in RANS solutions, as discussed in Jesus *et al.* (2013). Therefore, the current results at $Re_\tau = 2000$ are suggesting that, besides the aspects related to flow separation, RANS models may also lack some of the physics present in APG regions, particularly those pertaining to turbulent kinetic energy production.

4. CONCLUDING REMARKS

The paper has presented LES results for the skin friction coefficient along the bottom wall of a two-dimensional bump in a channel. Calculations performed at $Re_\tau = 617$ show a good comparison with DNS computations. At the rear portion of the bump, C_f distributions obtained with LES present similar patterns in higher Reynolds numbers, $Re_\tau = 950$ and 2000, even when there is no flow separation. Particularly, a sharp decrease and recovery of C_f is observed in the APG regions at all Reynolds numbers studied here.

Two-equation eddy-viscosity models and a seven-equation RSM model, for the RANS equations, are also studied and compared with the LES and DNS solutions. RANS-calculated skin friction coefficients almost perfectly matched DNS or LES results in zero or favorable pressure gradient regions. In regions of adverse pressure gradients, however, it is found that none of the RANS models considered is able to reproduce the behavior observed in LES or DNS calculations. The seven-equation RSM model studied has a better performance when compared to standard two-equation eddy-viscosity models, particularly in the higher Reynolds number range here analyzed. Hence, the results in the paper seem to indicate that the RANS models are not really able to capture the full physics of turbulence related with adverse pressure gradients.

The results obtained at $Re_\tau = 2000$ indicate that the inability of RANS models in describing skin-friction coefficient distributions in APG regions is not only related to prediction of flow separation and reattachment. Since this test case actually does not have flow separation, and the RANS results follow the general trends observed at lower Reynolds

L.A.C.A. Schiavo, A.B. Jesus, W.R. Wolf and J.L.F. Azevedo
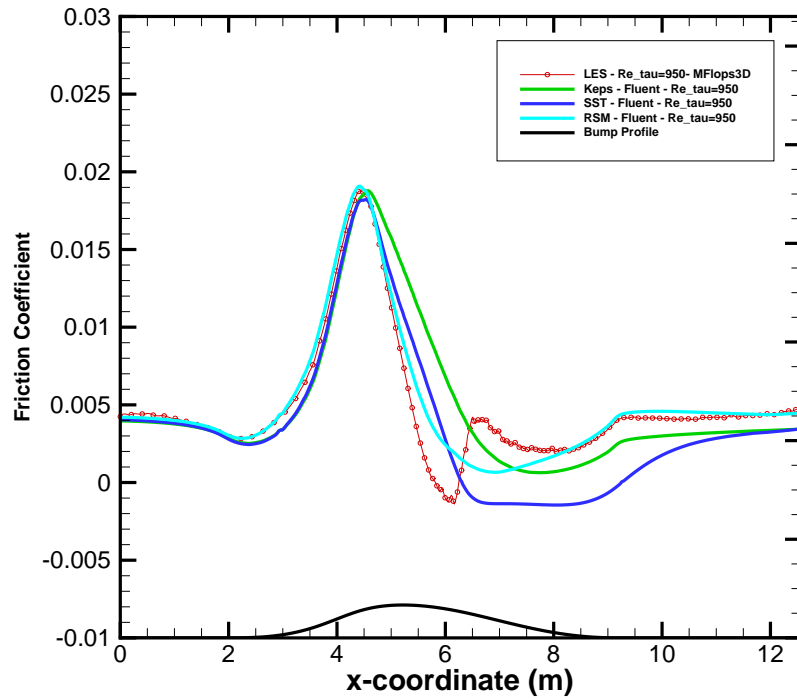A Study of Turbulent Flows in 2-D Channels Using Large Eddy Simulations

Figure 7. Bottom wall friction coefficient distributions. RANS: $Re_\tau = 950$; LES: $Re_\tau = 950$.
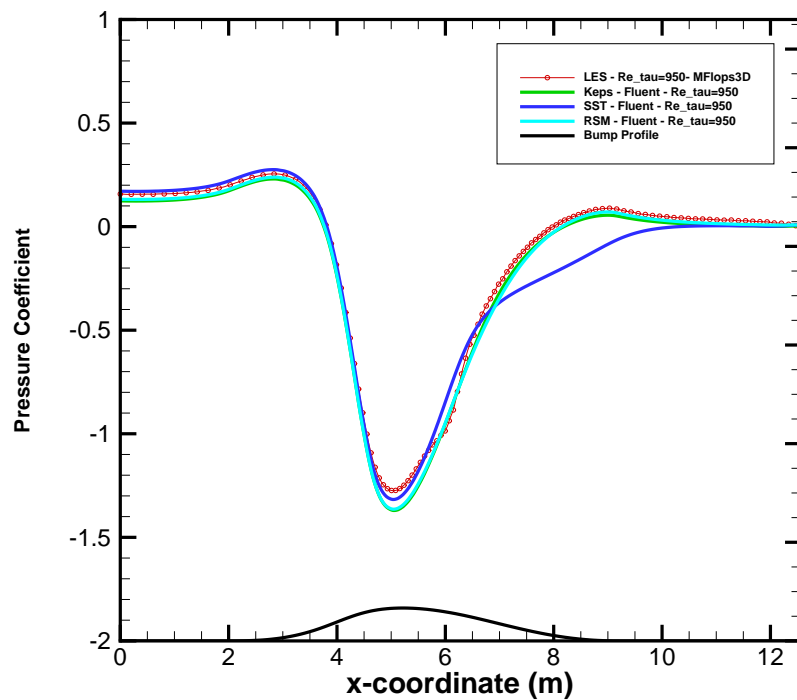

Figure 8. Bottom wall pressure coefficient distributions. RANS: $Re_\tau = 950$; LES: $Re_\tau = 950$.
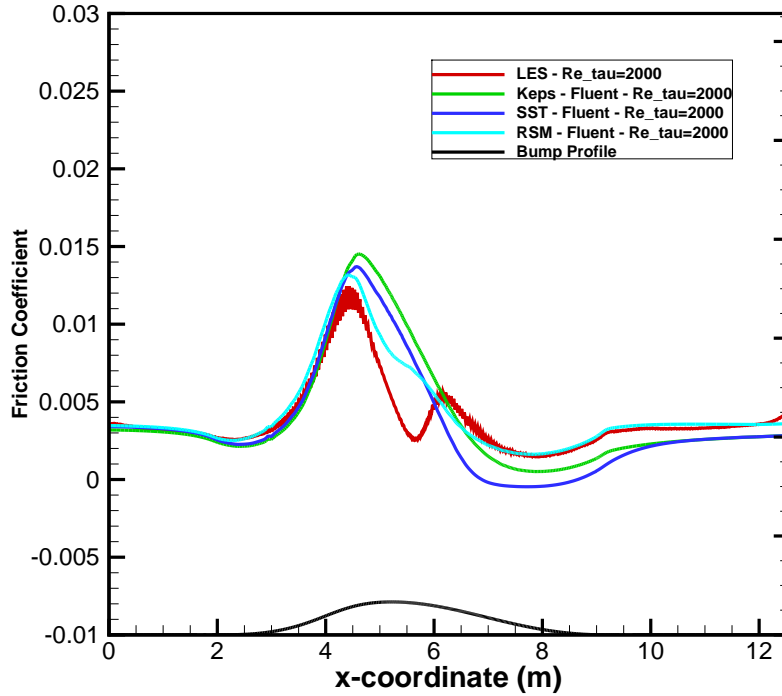
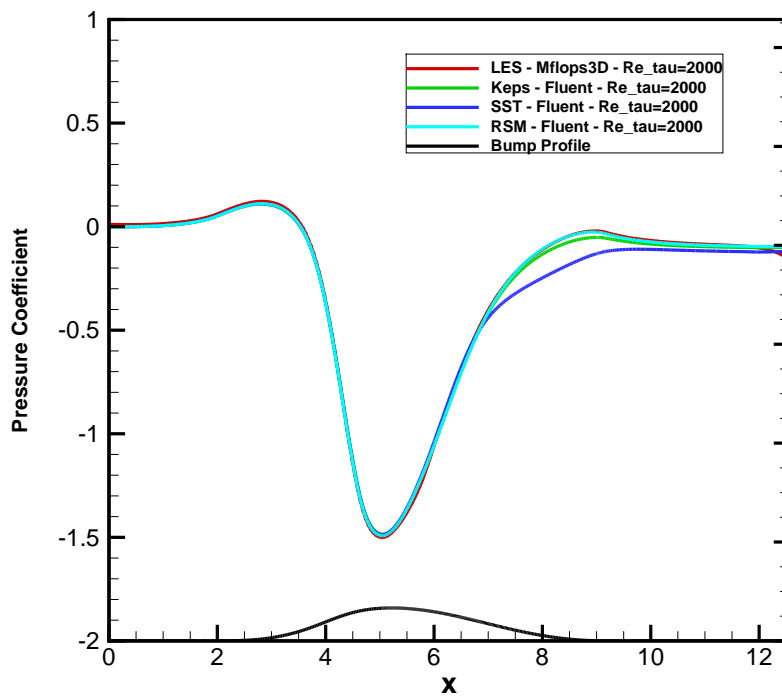Figure 9. Bottom wall friction coefficient distributions for RANS and LES calculations at $Re_\tau = 2000$.

Figure 10. Bottom wall pressure coefficient distributions for RANS and LES calculations at $Re_\tau = 2000$.

numbers, there seems to be enough evidence that the prevailing physical mechanism is associated with the existence of an adverse pressure gradient region. The observed behavior seems to be related to the fact that the RANS models do not correctly describe the production and evolution of the turbulent kinetic energy close to the walls in adverse pressure gradient regions.

5. ACKNOWLEDGEMENTS

6. REFERENCES

Ansys Fluent, 2011. *ANSYS FLUENT Theory Guide Release 14.0*. ANSYS, Inc.

Jesus, A.B., Azevedo, J.L.F. and Laval, J.P., 2013. "Large eddy simulations and RANS computations of adverse pressure gradient flows". In AIAA Paper No. AIAA 2013-0267*, 51st AIAA Aerospace Sciences Meeting including the New Horizons Forum and Aerospace Exposition*. Grapevine, TX.

Jeyapaul, E. and Rumsey, C., 2013. "Analysis of highly-resolved simulations of 2-D humps toward improvement of second-moment closures". In AIAA Paper No. AIAA 2013-0684*, 51st AIAA Aerospace Sciences Meeting including the New Horizons Forum and Aerospace Exposition*. Grapevine, TX.

Kuban, L., Laval, J.P., Elsner, W., Tyliszcak, A. and Marquillie, M., 2012. "LES modeling of converging-diverging turbulent channel flow". *Journal of Turbulence*, Vol. 16, No. N11, pp. 1–19.

Launder, B.E. and Shima, N., 1989. "Second-moment closure for the near-wall sublayer: Development and application". *AIAA Journal*, Vol. 27, No. 10, pp. 1319–1325.

Marquillie, M. and Ehrenstein, U., 2003. "On the onset of nonlinear oscillations in a separating boundary-layer flow". *Journal of Fluid Mechanics*, Vol. 490, pp. 169–188.

Marquillie, M., Ehrenstein, U. and Laval, J.P., 2011. "Instability of streaks in wall turbulence with adverse pressure gradient". *Journal of Fluid Mechanics*, Vol. 681, pp. 205–240.

Marquillie, M., Laval, J.P. and Dolganov, R., 2008. "Direct numerical simulation of separated channel flows with a smooth profile". *Journal of Turbulence*, Vol. 9, No. 1, pp. 1–23.

Menter, F.R., Kuntz, M. and Langtry, R., 2003. "Ten years of industrial experience with the SST turbulence model". In *Turbulence, Heat and Mass Transfer 4*, Begell House, Inc.

Nicoud, F. and Ducros, F., 1999. "Subgrid-scale stress modelling based on the square of the velocity gradient tensor". *Flow, Turbulence and Combustion*, Vol. 62, pp. 183–200.

Shih, T.H., Liou, W.W., Shabbir, A., Yang, Z. and Zhu, J., 1995. "A new $k - \epsilon$ eddy-viscosity model for high Reynolds number turbulent flows - model development and validation". *Computers and Fluids*, Vol. 24, No. 3, pp. 227–238.

Stanislas, M., Jimenez, J. and Marusic, I., eds., 2009. *Progress in Wall Turbulence: Understanding and Modeling*, ERCOFTAC. Springer.

7. RESPONSIBILITY NOTICE

The authors are the only responsible for the printed material included in this paper.